universe

MDPI

Article

Continuous Gravitational Wave Emissions from Neutron Stars with Pinned Superfluids in the Core

Brynmor Haskell [1,*], Marco Antonelli [2] and Pierre Pizzochero [3]

[1] Nicolaus Copernicus Astronomical Center of the Polish Academy of Sciences, ul. Bartycka 18, 00-716 Warszawa, Poland
[2] CNRS/in2p3 and LPC Caen, 14050 Caen, France
[3] Dipartimento di Fisica Aldo Pontremoli, Università degli Studi di Milano and INFN, Via Celoria 16, 20133 Milan, Italy
* Correspondence: bhaskell@camk.edu.pl

Abstract: We investigate the effect of a pinned superfluid component on the gravitational wave emissions of a rotating neutron star. The pinning of superfluid vortices to the flux-tubes in the outer core (where the protons are likely to form a type-II superconductor) is a possible mechanism to sustain long-lived and non-axisymmetric neutron currents in the interior, which break the axial symmetry of the unperturbed hydrostatic configuration. We consider pinning-induced perturbations to a stationary corotating configuration and determine the upper limits on the strength of gravitational wave emissions due to the pinning of vortices with a strong toroidal magnetic field of the kind predicted by recent magneto-hydrodynamic simulations of neutron star interiors. We estimate the contributions to gravitational wave emissions from both the mass and current multipole generated by the pinned vorticity in the outer core and find that the mass quadrupole can be large enough for gravitational waves to provide the dominant spindown torque in millisecond pulsars.

Keywords: neutron stars; pulsars; superconductivity; superfluidity; continuous gravitational waves

check for updates

Citation: Haskell, B.; Antonelli, M.; Pizzochero, P. Continuous Gravitational Wave Emissions from Neutron Stars with Pinned Superfluids in the Core. *Universe* **2022**, *8*, 619. https://doi.org/10.3390/universe8120619

Academic Editors: Ignazio Bombaci and Rosa Poggiani

Received: 20 October 2022
Accepted: 18 November 2022
Published: 24 November 2022

Publisher's Note: MDPI stays neutral with regard to jurisdictional claims in published maps and institutional affiliations.

Copyright: © 2022 by the authors. Licensee MDPI, Basel, Switzerland. This article is an open access article distributed under the terms and conditions of the Creative Commons Attribution (CC BY) license (https://creativecommons.org/licenses/by/4.0/).

1. Introduction

The detection of Neutron Star (NS) binary inspirals [1] has opened the field of Gravitational Wave (GW) NS astronomy [2], allowing us to place constraints on the internal composition of the star and nuclear parameters of dense matter, e.g., [3–5]. Further advances in our understanding of NS physics are expected to come as new detections are made in the next observation run (O4) of the LIGO, Virgo and KAGRA network; see [6,7] for a recent perspective on the topic. In particular, the instruments are now sensitive enough that one can hope to detect not only GW signals from compact object mergers but also Continuous Wave (CW) signals [8]. These signals are regular, long-lived signals for which galactic rotating NSs are some of the most likely sources [9–11].

One of the main emission mechanisms that has been suggested for CWs from rotating NSs is the presence of a so-called "mountain", i.e., a quadrupolar deformation that couples to the gravitational field and can lead to GW emissions at both the stellar rotation frequency and at twice the rotation frequency—essentially a GW pulsar. The mountain is sustained either by crustal rigidity [12] or by the magnetic field of the star [13]; see also [14] and the references therein.

Researchers have suggested that the observed spin frequencies of accreting NSs in Low-Mass X-Ray Binaries (LXMBs) may be set by the equilibrium between spin-up torques due to accretion and spin-down torques due to GW emissions from mountains created from the asymmetric spread of the accreted material [15,16]. Furthermore, observations of millisecond radio pulsars, which are thought to be old recycled NSs, spun up to millisecond rotation periods (P) by accretion in an LMXB, show that there appears to be a cut-off in the allowed parameter space for their evolution in the $P - \dot{P}$ diagram [17].

Remarkably, the cut-off can be explained by the presence of a residual deformation with an ellipticity of $\epsilon \approx 10^{-9}$, which leads to GW emissions and causes the systems to evolve out of the excluded region. Research suggested (see [17]) that, if the core of the star is superconducting, there is a buried magnetic field B on the order of $B \approx 10^{12}$ G, while such a configuration is theoretically possible, it is at the upper limit of what is plausible, given the weak external fields of $B \approx 10^{8}$ G inferred in these systems.

In this paper, we shall therefore consider a different mechanism to understand whether it may play a role in CW emission in rapidly rotating NSs and whether it could explain the distribution of millisecond pulsars in the $P - \dot{P}$ diagram. As we previously mentioned, the protons in the interior of a mature NS are expected to be superconducting, and the neutrons will also be in a superfluid state. The neutron superfluid rotates by means of quantised vortices, which can interact with the normal component of the star, thereby, giving rise to both a dissipative coupling (the so-called mutual friction [18–20]) and, if the coupling is strong enough, to pinning to either ions in the crustal lattice [21] or magnetic field flux-tubes in core of the NS [22].

Vortex pinning is at the heart of most pulsar glitch models, which build upon the notion that a pinned superfluid cannot expel vorticity and, thus, cannot spin-down and instead stores angular momentum. Eventually, once the lag between the superfluid and the normal component becomes overly large, hydrodynamical lift forces can overcome the pinning forces, and there is a sudden exchange of angular momentum, i.e., a glitch [23,24]. The same concept may also be used in reverse to explain anti-glitches in spinning-up pulsars [25,26].

The pinning of a large number of vortices in the crust of a neutron star is generally expected to lead to non-axisymmetric perturbations of the fluid [27,28] and, thus, possibly to GW emissions, while no signal has been detected in post-glitch searches to date [29–31], some microscopic models of vortex motion in NS crusts predict signals that may be detectable in the near future [28,32–34].

While most glitch models focus on pinning to the crustal lattice [23], recent observations of large glitch activity in the the Vela pulsar combined with theoretical calculations of the entrainment parameter in the crust [35,36] have shown that the moment of inertia of the crust is not sufficient to explain the amount of spin-down reversed by glitches over time [37,38]; see also [39] for a revision of the original theoretical argument and inclusion of statistical uncertainty on glitch-activity estimates. This points towards a picture in which part of the extra angular momentum transferred in a glitch should be stored in the core, a conclusion that is alsp consistent with simplified models of the maximum glitch sizes in combination with the average activity [40], post-glitch relaxation [41], and analysis of the spin-up in 2016 Vela glitch [42].

In particular, the presence of a stronger toroidal field in the interior of the star, which leads to regions of strong pinning of vortices to superconducting flux-tubes (see [22,43] and the references therein), could explain some glitch features [44,45], such as glitch overshoots [42,46]. From the theoretical point of view, the situation is unclear, as models have been constructed with toroidal components of the field that can be up to two orders of magnitude stronger than the inferred exterior dipole [47]; however, the inclusion of superconductivity in the models generally leads to the expulsion of the toroidal flux to the crust of the star [48,49], restricting the amount of angular momentum that could be stored in the outer core to power a glitch.

While further GRMHD modelling is likely to shed light on the internal configuration of the field (see, e.g., [50] for recent models), in this paper, we take as a starting point the observational clues that vortex pinning to flux-tubes may be present in the core and may interact with each other [51], and we investigate the consequences for GW emission. In particular, we consider models with strong toroidal fields, such as those proposed by [52], in which the magnetic axis is possibly inclined with respect to the rotation axis. This breaks the axisymmetry of the problem and leads to non-axisymmetric regions of strong pinning in which vortices may accumulate and lead to velocity perturbations and a mass current quadrupole, thereby, resulting in CW emissions.

Researchers demonstrated [53] that, in the presence of a pinned superfluid, a deformed rotating NS may emit GWs at both the rotation frequency and twice the rotation frequency; hence, we will consider both emissions in the $l = 2, m = 1$ and $l = 2, m = 2$ harmonic in our model.

The paper is organised as follows: In Section 2, we introduce the basic two-fluid formalism and the hydrodynamic force associated with the presence of pinned vorticity. The relation between vortex pinning and the magnetic field configuration is outlined in Section 3 together with the geometry of the pinning region. Section 4 is devoted to discussing stationary perturbations around a global equilibrium solution of the equations introduced in Section 1. The formalism needed to extract the gravitational wave emissions associated with these stationary perturbations is given in Section 5. In Section 6, we present our numerical estimates for the continuous gravitational wave emissions due to a triaxial deformation of the star induced by the presence of pinning regions. We summarize our findings in Section 7.

2. Setting the Stage: Hydrodynamic Perturbations

As a first step, we present the formalism to describe the perturbed structure of a superfluid NS, modelled in terms of two components, a 'proton' component (in reality, a charge-neutral fluid of protons and electrons) and a superfluid 'neutron' component (see [54,55] for a review of the formalism).

In a rotating frame of constant angular velocity vector Ω and in the limit of slow chemical reactions, the equations of motion for the two species are:

$$D_{\mathrm{x}}\, p_i^{\mathrm{x}} + \varepsilon_{\mathrm{x}} v_j^{\mathrm{yx}}\, \nabla_i\, v_{\mathrm{x}}^j + \nabla_i \Phi_{\mathrm{x}} + 2\,\epsilon_{ijk}\Omega^j v_{\mathrm{x}}^k = f_i^{\mathrm{x}} \tag{1}$$

$$\partial_t \rho_{\mathrm{x}} + \bigtriangledown^j (\rho_x v_j^x) = 0 \tag{2}$$

where the chemical index $\mathrm{x} = n$ refers to the neutrons; $\mathrm{x} = p$ is used for the "proton" component; and the index y is used for the species other than x, e.g., $\mathrm{y} = p$ if $\mathrm{x} = n$. The vectors v_{x}^i and p_i^{x} are, respectively, the kinematic velocity field and the momenta per unit mass of the x species. $v_i^{\mathrm{yx}} = v_i^{\mathrm{y}} - v_i^{\mathrm{x}}$ is a shorthand for the relative velocity between the two components (also referred to as 'lag") and $D_{\mathrm{x}} = \partial_t + v_{\mathrm{x}}^j \nabla_j$. On the left-hand side, f_i^{x} is the mutual friction force per unit mass, which is a hydrodynamic coupling between the two species that arises when many quantized vortices are present in the local fluid element [19,20]. The effective potential Φ_{x} accounts for gravity (via the gravitational potential Φ), pressure gradients (via the chemical potential per unit mass $\tilde{\mu}_x$), and centrifugal force:

$$\Phi_{\mathrm{x}} = \Phi + \tilde{\mu}_x - |\Omega \times r|^2/2\,. \tag{3}$$

The two thermodynamic quantities that appear in Equation (1) (namely, $\tilde{\mu}_{\mathrm{x}}$ and ε_{x}) represent the specific chemical potential and the entrainment parameter of each species (see [56] for a formal discussion of superfluid thermodynamics). In (1), the non-dissipative entrainment coupling between the two fluids enters also into the definition of the two specific momenta p_i^{x}; see, e.g., [36,55],

$$p_i^{\mathrm{x}} \;=\; v_i^{\mathrm{x}} + \varepsilon_{\mathrm{x}}\, v_i^{\mathrm{yx}} \;=\; (1-\varepsilon_{\mathrm{x}}) v_i^{\mathrm{x}} + \varepsilon_{\mathrm{x}} v_i^{\mathrm{y}} \quad \text{for} \quad \mathrm{y} \neq \mathrm{x}\,. \tag{4}$$

All these quantities are local macroscopic variables: the momentum p_i^n is the average momentum per unit mass of a superfluid element that contains several quantized vortex lines; see, e.g., [20]. Since the number of vortices is a physical quantity independent of the frame of reference, to calculate the mutual friction, we must use the the absolute vorticity—namely, the macroscopic smooth field defined as

$$\omega^i \;=\; \epsilon^{ijk}\, \nabla_j\, p_k^n \;+\; 2\,\Omega^i\,. \tag{5}$$

The unit vector $\hat{\omega} = \omega/|\omega|$ defines a preferred direction, along which the quantized vortex lines are (on average) locally aligned. When this is the case, the vortex-mediated mutual friction reads [19,20]

$$f_i^{\rm x} = \frac{\rho_n}{\rho_x}\left(\mathcal{B}'\,\epsilon_{ijk}\omega^j v_{\rm xy}^k + \mathcal{B}\,\epsilon_{iab}\hat{\omega}^a\epsilon_{blm}\omega^l v_{\rm xy}^m\right), \tag{6}$$

where $\mathcal{B}'$ and $\mathcal{B}$ are two dimensionless parameters that encode the physics of the complex dissipation processes at the vortex scale; see [20,57,58] and the references therein. As shown in the kinetic simulations of fluid elements with many vortices, the parameters $\mathcal{B}'$ and $\mathcal{B}$ depend on the state of motion of the vortex ensemble [20]: for perfect pinning (as we will consider in the following), we are in the dissipationless limit, where $\mathcal{B}' = 1$ and $\mathcal{B} = 0$—namely,

$$f^n = \omega \times v_{np} \qquad f^p = -\frac{\rho_n}{\rho_p}\,\omega \times v_{np}\,. \tag{7}$$

3. Magnetic Field and Pinning

Below temperatures of approximately 10^9 K, the protons in the core of a NS are expected to form a type-II superconductor [36,55], in which the magnetic field is organised in flux-tubes (see [59] for the possibility of having a type-I superconductor). Superfluid neutron vortices are magnetised as a consequence of the entrainment effect, and there is thus an energy penalty associated with cutting through a magnetic flux-tube [22,51]. This interaction effectively leads to vortices pinning to flux-tubes, below a relative velocity (for a core magnetic field strength B)

$$w \approx 1.5 \times 10^4 \left(\frac{B}{10^{12}\,\mathrm{G}}\right)^{1/2} \mathrm{cm/s} \tag{8}$$

above which hydrodynamical lift forces will unpin the vortices [60]; see also [43]. This estimate is valid for the so-called S-wave superfluid, namely, where Cooper pairs of neutrons are in the spin singlet state [61]. If, on the other hand, neutron pairing is in the P-wave channel (i.e., neutrons form pairs in the triplet state), then the pinning strength is expected to be suppressed, thereby, lowering the estimate of the critical lag in (8); see [62].

As can be seen from (8), the strength of the pinning therefore depends on the large scale structure of the magnetic field, essentially because this dictates the flux-tube density. The equilibrium structure of the magnetic field in the interior of a NS is still an open problem [63]; nevertheless, several models have been developed, and there is a general consensus that, to be stable, the field must have a twisted-torus configuration, in which a strong interior toroidal component stabilises the poloidal component of the field, which stretches outside the star [47,64,65].

The relative strength of the toroidal field is particularly interesting as, while many models require this component to be somewhat weaker (roughly an order of magnitude) than the poloidal component [48,49], there are several models that predict stronger toroidal components in the interior [52,66], which would lead to regions of strong vortex-flux-tube pinning [22].

From the observational side, there is some indication that a pinned superfluid must exist in the core of at least the Vela pulsar to explain the large fraction of spin-down that is inverted by its glitches over time (the activity; see the discussion in [39]) but also to explain the difference in post-glitch relaxation with respect to the Crab pulsar [41] and the behaviour of moderately active pulsars displaying glitches of large size, such as PSR J1341-6220 [40].

In order to calculate the strongest GW signal, we consider the case of an orthogonal rotator in which the magnetic field axis is perpendicular to the rotation axis. This may be expected to be the case in a newly born NS but not throughout the entire population of pulsars. It is nevertheless a useful upper limit. In this case, vortices (which we assume to

be straight on a mesoscopic scale) are aligned to toroidal flux-tubes and will be strongly pinned when they overlap with the closed line region and will be essentially free outside.

In the following, we consider an approximation to the models of [52], which maximises the strength of the toroidal component in the core of the star: the closed field-line region in which the toroidal field resides stretches from about $r_{in} = 0.4R_*$ to $r_{out} = 0.8R_*$ and is symmetric around the equatorial plane. Therefore, for definiteness, we will assume that the vortices are pinned in a region between r_{in} and r_{out}, $\theta_{min} = \pi/2 - \arccos(r_{in}/r_{out})$ and $\theta_{max} = \pi/2 + \arccos(r_{in}/r_{out})$ and $\phi_{min} = 2\pi - 0.08\pi$ and $\phi_{max} = 0.08\pi$ as sketched in Figure 1.

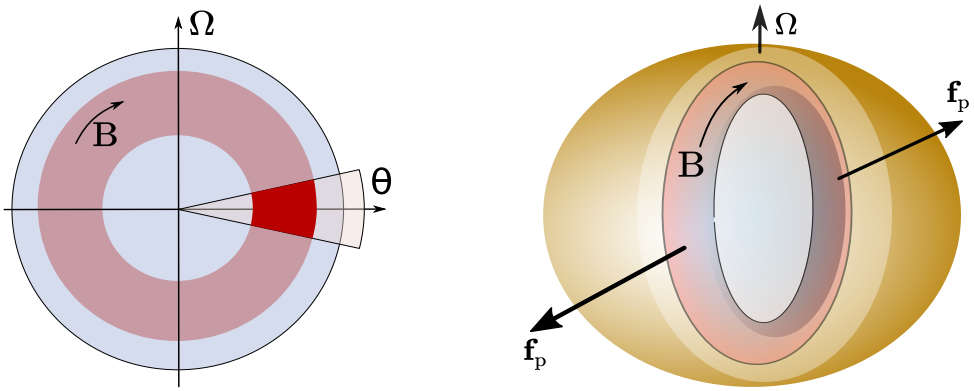

Figure 1. Left: Lateral view of our simplified configuration, in which the neutron star has been sliced along the vertical plane containing the toroidal magnetic field region (its width goes from about $0.4R_*$ to $0.8R_*$). The two axes are the rotation axis of the neutron star aligned with the angular velocity Ω and the $(\theta = \pi/2, \phi = 0)$, while the dark red region corresponds to the strong pinning region as indicated in the text. **Right**: Cartoon of the triaxial deformation induced by the presence of pinned vortices in the two (diametrically opposed) strong pinning regions. For perfect pining, the force $\mathbf{f}_p$ in (7) is directed outwards when the superfluid spins faster than the normal component. Both sketches are not to scale.

4. Perturbation Equations for the Pinned Configuration

The general equations governing the perturbations of the hydrodynamic model defined by (1), (2) and (6) are derived in [67]. Here, to estimate the effect of a pinned superfluid on the stellar structure and internal flow, we can consider a less general setting in which the small velocity lag given by the pinning of the neutron vortices to the superconducting flux-tubes is treated as a small perturbation of a background configuration in which the two fluids are corotating.

We consider a constant density background model where neutrons and protons are locked together, while, in the strong pinning region sketched in Figure 1, we have $\mathcal{B}' = 1$, and there is a rotational velocity lag given by (8), such that one has $\delta v^i_p = 0$ and

$$\delta v^\phi_n = w\,\Theta(r - r_{min})\Theta(r_{max} - r)\Theta(\theta - \theta_{min})\Theta(\theta_{max} - \theta)\Theta(\phi - \phi_{min})\Theta(\phi_{max} - \phi)\,, \quad (9)$$

where Θ is the unit step function. In principle, only the part of this region in which the S-wave superconductor and S-wave superfluid coexist should be considered. Therefore, the exact extent of the pinning region sketched in Figure 1 as well as the strength of pinning [22] both depend on the exact stratification of the star and, hence, on the equation of the state for nuclear matter (and its consistent dependence of the pairing gaps on density; see, e.g., [61]) as well as on the mass of the star.

In fact, nuclear models that favour P-wave pairing of neutrons in the outer core are expected to greatly shrink the pinning region to only the lowest-density part of the outer core, as pinning between flux-tubes and topological defects in the P-wave superfluid is likely ineffective [62]. However, since our goal is to provide an upper-limit estimate, we will consider the full region in Figure 1 as effective, employing there the estimate for pinning

between fluxtubes and S-wave superfluid vortices as discussed by [60]; see also [43]. In a more realistic scenario, both the extent of the pinning region as well as the pinning strength may be reduced[1].

For simplicity, and since our goal is to provide a first estimate, we also consider incompressible perturbations ($\delta\rho = 0$) and the Cowling approximation ($\delta\Phi = 0$).

Following [68], we can write the perturbed equilibrium equations for the fluids in terms of co-moving and counter-moving variables, which gives, for the perturbations of the density and velocity,

$$\rho\delta v_j = \rho_n \delta v_j^n + \rho_{\rm p}\delta v_j^p = \rho_n \delta v_j^n \tag{10}$$

$$\delta w_j = \delta v_j^p - \delta v_j^n = -\delta v_j^n\,, \tag{11}$$

which are valid for constant density incompressible fluids with $\delta v_p^i = 0$. The continuity equations take the form (assuming time-independent perturbations):

$$\nabla_j(\rho\delta v^j) = \nabla_j(\rho_{\rm n}\delta v_n^j) = 0 \tag{12}$$

$$\frac{1}{\rho}\nabla_j[x_p(1-x_p)\rho\delta w^j] + \delta v_j \nabla^j x_p = 0, \tag{13}$$

and we remind the reader that we are considering constant density ρ and proton fraction $x_{\rm p}$, and incompressible fluids ($\delta\rho = 0$) as well as the Cowling approximation ($\delta\Phi = 0$). Finally, one has the momentum equations for the co-moving perturbations:

$$\nabla^i\delta\Phi + \frac{\nabla^i\delta p}{\rho} + 2\epsilon^{ijk}\Omega_j w_k = 0 \tag{14}$$

with $\nabla^i p = \rho_{\rm n}\nabla^i\tilde{\mu}_{\rm n} + \rho_{\rm p}\nabla^i\tilde{\mu}_{\rm p}$ and, for the counter-moving perturbations,

$$\nabla^i(\delta\mu_{\rm p} - \delta\mu_{\rm n}) + 2\bar{\mathcal{B}}'\epsilon_{ijk}\Omega^j\delta w^k - \bar{\mathcal{B}}\epsilon_{ijk}\hat{\Omega}^k\epsilon^{klm}\Omega_l\delta w_m = 0 \tag{15}$$

where $\bar{\mathcal{B}} = \mathcal{B}/x_p$ and $\bar{\mathcal{B}}' = 1 - \mathcal{B}'/x_p$. We can see immediately that, for a velocity perturbation of the form in (9), the total and countermoving continuity Equations (12) and (13) are satisfied in all the stars, except locally at the edge of the pinning domain due to the sharp boundaries defined by the Heaviside step functions present in (9). They are, however, satisfied in an average sense if one integrates over a volume containing the boundary. Finally, from (14) and (15), one can calculate the pressure perturbations δp and chemical imbalance $\delta\mu_{\rm p} - \delta\mu_{\rm n}$ due to pinning.

5. Continuous Wave Emission

In NS interiors large non axisymmetric mass and velocity perturbations can couple to the background metric and lead to the emission of GWs: the emissions can be either continuous (e.g., in the case of long-lived "mountains") or burst-like as expected from pulsar glitch events [32,33,69,70]. The GW strain h_{TT} is generally described in terms of a multipole expansion, where the leading order is the $l = 2$ multipole (the quadrupole), such that:

$$h_{ij}^{TT} = \frac{G}{c^4 r}\sum_{l=2}^{\infty}\sum_{j=-l}^{l}\left(\frac{d^l}{(dt)^l}I_{lm}(t-r)T^{E2}_{lm,ij} + \frac{d^l}{(dt)^l}S_{lm}(t-r)T^{B2}_{lm,ij}\right) \tag{16}$$

where T^{E2} and T^{B2} are electric and magnetic tensor spherical harmonics, and I and S are generalized mass and current multipole moments [71], such that, for the leading order ($l = 2$), the terms are

$$I_{2m} = \frac{16\sqrt{3}\pi}{15}\int \tau_{00} Y^*_{2m} r^2 d^3x \tag{17}$$

$$S_{2m} = \frac{32\sqrt{2}\pi}{15}\int (-\tau_{0j}) Y^{B*}_{22,j} r^2 d^3x, \tag{18}$$

respectively, where τ is the stress-energy tensor. Y are scalar, and Y^B are magnetic vector spherical harmonics. As a first step, we consider an incompressible fluid, which naturally leads to a vanishing mass quadrupole under our working hypotheses. This is a common approximation as this is generally not thought to be the dominant contribution for superfluid flows [33]. In the following, we will go beyond this approximation and show that it can be the dominant contribution for the model we consider. For slow motion, we have, for the mass quadrupole:

$$\tau^{00} \approx \rho \tag{19}$$

and, for the current multipoles:

$$\tau^{0j} \approx \frac{1}{c}(\rho_{\rm n} v^j_{\rm n} + \rho_{\rm p} v^j_{\rm p})\,. \tag{20}$$

If we assume a rigidly rotating background in which the two fluids (the superfluid and the normal component) are corotating, the only contribution to the current quadrupole is due to he perturbations in the superfluid neutron velocity in the pinned regions. We can therefore write:

$$S_{2m} = \frac{32\pi}{15\sqrt{3}c}\int Y^*_{2m} r^2 x^i \epsilon_{ijk} \nabla^j (\rho_{\rm n} \delta v^k_{\rm n}) d^3x \tag{21}$$

The resulting gravitational wave luminosity takes the form:

$$\frac{dE_{gw}}{dt} = \frac{G}{32\pi c^5}\sum_m |\dddot{S}_{2m}|^2 + |\dddot{I}_{2m}|^2 \tag{22}$$

Clearly, for our uniform density and incompressible model, $\delta\rho = 0$, and $\tau^{00} = \rho$ is spherically symmetric; thus, the mass quadrupole terms vanish, and the current multipole emission dominates. Nevertheless, in a realistic neutron star, compressibility will lead to density perturbations associated with the velocity perturbations that are associated with the pinning. In order to estimate these, in the following, we make the approximation that

$$\delta\rho \approx \frac{\delta p}{c_s^2} \tag{23}$$

where c_s is the (constant) speed of sound, and we obtain δp by solving the total Euler equation in (14) leading to

$$\delta\rho = -2\Omega w \rho r c_s^{-2} \sin\theta\,. \tag{24}$$

We stress again that this is an order of magnitude estimate, as the problem we are solving is incompressible.

6. Results

We evaluate the integrals in (21) for the setup described in Section 3, assuming, therefore, a perturbation in the neutron velocity only in the strong pinning region. Given the equatorial symmetry, the $l = 2, m = 0$ and $l = 2, m = 2$ components of the current multipole vanish, and the leading order contribution is the $l = 2, m = 1$ multipole (similarly to the case examined by [33] for vortex avalanches). However, also in this case, the symmetry we assumed in the equatorial plane for the two portions of the pinning region, leads to the $m = 1$ contribution vanishing so that the $l = 2$ current multipole vanishes, i.e., $S_{2m} = 0$.

In realistic MHD simulations, however, the field configuration is significantly more complex than in our simple setup [65] as required also by pulse profile modelling with the NICER X-Ray telescope [72,73]. If the strong pinning regions are not symmetric in the

equatorial plane, there will thus be small contributions to the S_{21} multipole—the strength of which will depend on the degree of asymmetry.

Let us also consider, however, the contribution to the the mass quadrupole I_{22} due to the density perturbations in the pinning region as estimated from (23). In this case, we obtain

$$I_{22} \approx -2 \times 10^{38} \left(\frac{B}{10^{12} G} \right)^{1/2} \left(\frac{\nu}{100\,\mathrm{Hz}} \right) \ \mathrm{g\ cm^2} \tag{25}$$

where ν is the rotation frequency of the star, and the GWs are emitted at 2ν. We evaluated our expression for a representative constant density of $\rho = 4 \times 10^{14}$ g/cm^3, corresponding to the pinning region of the outer core. However, in our model, the pinning region extends throughout the outer core in a range of densities from $\rho \approx 2 \times 10^{14}$ g/cm^3 to $\rho \approx 10^{15}$ g/cm^3.

Our estimate is approximate and likely to be an upper limit due to the extrapolation from the incompressible case. It is clear, nevertheless, that the mechanism should be considered in more detail as this could explain the residual ellipticity inferred by [17] in the millisecond radio pulsars. Furthermore, the scaling with the strength of the magnetic field B is weaker than in the case of standard deformations due to the Lorentz force. In this case, one would have [48]

$$I_{22}^{L} \approx 3 \times 10^{37} \left(\frac{B}{10^{12} G} \right) \left(\frac{H_{c1}}{10^{16} G} \right) \ \mathrm{g\ cm^2} \tag{26}$$

where H_{c1} is the lower critical field of the type-II proton superconductor [48,74,75]. We see that the weaker scaling with the surface field strength B of the result for a pinned superfluid in (25) means that, even in the case of a weaker buried field on the order of $B \approx 10^9$ G, as is the expected to be the case in the millisecond radio pulsar population [76], one would still expect $\epsilon \approx 5 \times 10^{-9}$, and possibly a weaker emission in the Y_{21} multipole, depending on the asymmetry of the field structure.

7. Summary and Conclusions

In this paper, we evaluated the strength of the mass and current quadrupoles for a rotating superfluid NS with a type-II superconducting core in which vortices pin to magnetic flux tubes in the region where the toroidal field is stronger. We considered the case of an orthogonal rotator in which the magnetic field geometry is a twisted torus and the extent of the closed field line region in which the toroidal component is located is defined in such a way as to approximate the results of [52].

This defines two opposite regions of the star in which neutron vortices are strongly pinned, and a large velocity lag can be sustained between the neutron superfluid and the 'normal' component of the star. We evaluated the current quadrupole associated with this velocity lag and the associated mass quadrupole due to the density perturbation in the pinned region, which necessarily arises to ensure mass continuity.

We found that, due to the symmetries that we assumed, the current quadrupole (the $l = 2, m = 1$ multipole) vanished; however, the mass quadrupole (the $l = m = 2$ multipole) did not and was sizable, thereby, leading to an ellipticity on the order of

$$\epsilon \approx -10^{-9} \left(\frac{B}{10^{8} G} \right)^{1/2} \left(\frac{\nu}{100\,\mathrm{Hz}} \right). \tag{27}$$

This estimate should be considered as an upper limit as we assumed incompressible perturbations, an idealized geometry for the magnetic field, and the most favourable case of an orthogonal rotator. The quadrupole we obtain is, however, in line with the order of magnitude estimates of Jones [28]. It is thus an interesting result as it describes that a physical mechanism may provide the ellipticity needed to explain the observed cut-off in the $P - \dot{P}$ diagram [17].

Furthermore, the scaling with $\sqrt{B}$, unlike the deformation caused by the Lorentz force, which scales as B [48], is interesting: it implies that, also for weaker fields (on the order of $B \approx 10^8 - 10^9$ G, more in line with what is expected for millisecond pulsars), one may still have $\epsilon \approx 10^{-9}$ without invoking buried fields on the order of $B \approx 10^{12}$ G, which makes it difficult to reconcile theoretical models with the lack of observation of strong GW-driven spin-down in the millisecond radio pulsars [76].

Being an upper limit, our estimate is, admittedly, based on some simplifying working assumptions as discussed in Section 4. Our simple treatment does not immediately make clear what are the roles of the specific properties of nuclear matter, such as the equation of state and the values, nature, and density dependence of the pairing gap. These effects are all indirectly encoded within the estimate of the pinning strength in (8) and the extent of the pinning region. Therefore, it will be interesting to further corroborate our upper limit on the GW emissions with more refined compressible models of the kind derived in [77], in which it is possible to test the roles of the equation of state and the finite compressibility of nuclear matter.

Author Contributions: Conceptualization, B.H.; methodology, B.H., M.A. and P.P.; software, B.H. and M.A.; validation, B.H., M.A. and P.P.; formal analysis, M.H. and M.A.; investigation, B.H., M.A. and P.P.; resources, B.H.; data curation, B.H. and M.A.; writing—original draft preparation, B.H., M.A. and P.P.; writing—review and editing, B.H., M.A. and P.P; visualization, M.A.; supervision, B.H. and P.P.; project administration, B.H.; funding acquisition, B.H. All authors have read and agreed to the published version of the manuscript.

Funding: B.H. acknowledges support from the Polish National Science Centre grants SONATA BIS 2015/18/E/ST9/00577 and OPUS 2019/33/B/ST9/00942.

Institutional Review Board Statement: Not applicable.

Informed Consent Statement: Not applicable.

Data Availability Statement: Not applicable.

Acknowledgments: Partial support was from PHAROS, COST Action CA16214.

Conflicts of Interest: The authors declare no conflict of interest.

Note

[1] Apart from the uncertainties regarding the extent of the S-wave gap for superfluidity, further reduction in the pinning strength may be due to the fact that the mutual orientation between a vortex and the fluxtubes is expected to fluctuate locally, thereby, giving rise to a decrease of the effective pinning force, similarly to what happens for vortices that are randomly oriented with respect to the principal axis of the Coulomb lattice in the inner crust [21].

References

1. Abbott, B.P. et al. [The LIGO Scientific Collaboration and Virgo Collaboration]. GW170817: Observation of Gravitational Waves from a Binary Neutron Star Inspiral. *Phys. Rev. Lett.* **2017**, *119*, 161101. [CrossRef] [PubMed]
2. Abbott, B.P. et al. [The LIGO Scientific Collaboration and Virgo Collaboration]. Multi-messenger Observations of a Binary Neutron Star Merger. *Astrophys. J. Lett.* **2017**, *848*, L12. [CrossRef]
3. Abbott, B.P. et al. [The LIGO Scientific Collaboration and Virgo Collaboration]. GW170817: Measurements of Neutron Star Radii and Equation of State. *Phys. Rev. Lett.* **2018**, *121*, 161101. [CrossRef]
4. Güven, H.; Bozkurt, K.; Khan, E.; Margueron, J. Multimessenger and multiphysics Bayesian inference for the GW170817 binary neutron star merger. *Phys. Rev. C* **2020**, *102*, 015805. [CrossRef]
5. Mondal, C.; Gulminelli, F. Can we decipher the composition of the core of a neutron star? *Phys. Rev. D* **2022**, *105*, 083016. [CrossRef]
6. Lasky, P.D. Gravitational wave astronomy. In *Multimessenger Astronomy in Practice: Celestial Sources in Action*; Filipović, M.D., Tothill, N.F.H., Eds.; IOP Publishing: Bristol, UK, 2021; pp. 1–9. [CrossRef]
7. Piccinni, O.J. Status and Perspectives of Continuous Gravitational Wave Searches. *Galaxies* **2022**, *10*, 72. [CrossRef]
8. Riles, K. Searches for Continuous-Wave Gravitational Radiation. *arXiv* **2022**, arXiv:2206.06447.
9. Lasky, P.D. Gravitational Waves from Neutron Stars: A Review. *Publ. Astron. Soc. Austr.* **2015**, *32*, e034. [CrossRef]

10. Glampedakis, K.; Gualtieri, L. Gravitational Waves from Single Neutron Stars: An Advanced Detector Era Survey. In *Physics and Astrophysics of Neutron Stars*; Rezzolla, L., Pizzochero, P., Jones, D.I., Rea, N., Vidaña, I., Eds.; Astrophysics and Space Science Library: Springer Cham, Switzerland, 2018; Volume 457, p. 673. [CrossRef]
11. Haskell, B.; Schwenzer, K. Isolated Neutron Stars. In *Handbook of Gravitational Wave Astronomy*; Bambi, C., Ed.; Springer Nature: Cham, Switzerland, 2022; p. 12. [CrossRef]
12. Bildsten, L. Gravitational Radiation and Rotation of Accreting Neutron Stars. *Astrophys. J. Lett.* **1998**, *501*, L89–L93. [CrossRef]
13. Bonazzola, S.; Gourgoulhon, E. Gravitational waves from pulsars: Emission by the magnetic-field-induced distortion. *Astron. Astrophys.* **1996**, *312*, 675–690.
14. Singh, N.; Haskell, B.; Mukherjee, D.; Bulik, T. Asymmetric accretion and thermal 'mountains' in magnetized neutron star crusts. *Mon. Not. R. Astron. Soc.* **2020**, *493*, 3866–3878. [CrossRef]
15. Ushomirsky, G.; Cutler, C.; Bildsten, L. Deformations of accreting neutron star crusts and gravitational wave emission. *Mon. Not. R. Astron. Soc.* **2000**, *319*, 902–932. [CrossRef]
16. Haskell, B.; Jones, D.I.; Andersson, N. Mountains on neutron stars: Accreted versus non-accreted crusts. *Mon. Not. R. Astron. Soc.* **2006**, *373*, 1423–1439. [CrossRef]
17. Woan, G.; Pitkin, M.D.; Haskell, B.; Jones, D.I.; Lasky, P.D. Evidence for a Minimum Ellipticity in Millisecond Pulsars. *Astrophys. J. Lett.* **2018**, *863*, L40. [CrossRef]
18. Mendell, G. Superfluid Hydrodynamics in Rotating Neutron Stars. II. Dissipative Effects. *Astrophys. J.* **1991**, *380*, 530. [CrossRef]
19. Andersson, N.; Sidery, T.; Comer, G.L. Mutual friction in superfluid neutron stars. *Mon. Not. R. Astron. Soc.* **2006**, *368*, 162–170. [CrossRef]
20. Antonelli, M.; Haskell, B. Superfluid vortex-mediated mutual friction in non-homogeneous neutron star interiors. *Mon. Not. R. Astron. Soc.* **2020**, *499*, 3690–3705. [CrossRef]
21. Seveso, S.; Pizzochero, P.M.; Grill, F.; Haskell, B. Mesoscopic pinning forces in neutron star crusts. *Mon. Not. R. Astron. Soc.* **2016**, *455*, 3952–3967. [CrossRef]
22. Alpar, M.A. Flux-Vortex Pinning and Neutron Star Evolution. *J. Astrophys. Astron.* **2017**, *38*, 44. [CrossRef]
23. Anderson, P.W.; Itoh, N. Pulsar glitches and restlessness as a hard superfluidity phenomenon. *Nature* **1975**, *256*, 25–27. [CrossRef]
24. Haskell, B.; Melatos, A. Models of pulsar glitches. *Int. J. Mod. Phys. D* **2015**, *24*, 1530008. [CrossRef]
25. Ducci, L.; Pizzochero, P.M.; Doroshenko, V.; Santangelo, A.; Mereghetti, S.; Ferrigno, C. Properties and observability of glitches and anti-glitches in accreting pulsars. *Astron. Astrophys.* **2015**, *578*, A52. [CrossRef]
26. Ray, P.S.; Guillot, S.; Ho, W.C.G.; Kerr, M.; Enoto, T.; Gendreau, K.C.; Arzoumanian, Z.; Altamirano, D.; Bogdanov, S.; Campion, R.; et al. Anti-glitches in the Ultraluminous Accreting Pulsar NGC 300 ULX-1 Observed with NICER. *Astrophys. J.* **2019**, *879*, 130. [CrossRef]
27. Ruderman, M. Crust-breaking by neutron superfluids and the Vela pulsar glitches. *Astrophys. J.* **1976**, *203*, 213–222. [CrossRef]
28. Jones, D.I. Gravitational waves from rotating strained neutron stars. *Class. Quantum Gravity* **2002**, *19*, 1255–1265. [CrossRef]
29. Keitel, D.; Woan, G.; Pitkin, M.; Schumacher, C.; Pearlstone, B.; Riles, K.; Lyne, A.G.; Palfreyman, J.; Stappers, B.; Weltevrede, P. First search for long-duration transient gravitational waves after glitches in the Vela and Crab pulsars. *Phys. Rev. D* **2019**, *100*, 064058. [CrossRef]
30. Abadie, J. et al. [The LIGO Scientific Collaboration]. Search for gravitational waves associated with the August 2006 timing glitch of the Vela pulsar. *Phys. Rev. D* **2011**, *83*, 042001. [CrossRef]
31. Abbott, R. et al. [The LIGO Scientific Collaboration]. Narrowband Searches for Continuous and Long-duration Transient Gravitational Waves from Known Pulsars in the LIGO-Virgo Third Observing Run. *Astrophys. J.* **2022**, *932*, 133. [CrossRef]
32. Bennett, M.F.; van Eysden, C.A.; Melatos, A. Continuous-wave gravitational radiation from pulsar glitch recovery. *Mon. Not. R. Astron. Soc.* **2010**, *409*, 1705–1718. [CrossRef]
33. Warszawski, L.; Melatos, A. Gravitational-wave bursts and stochastic background from superfluid vortex avalanches during pulsar glitches. *Mon. Not. R. Astron. Soc.* **2012**, *423*, 2058–2074. [CrossRef]
34. Melatos, A.; Douglass, J.A.; Simula, T.P. Persistent Gravitational Radiation from Glitching Pulsars. *Astrophys. J.* **2015**, *807*, 132. [CrossRef]
35. Chamel, N. Neutron conduction in the inner crust of a neutron star in the framework of the band theory of solids. *Phys. Rev. C* **2012**, *85*, 035801. [CrossRef]
36. Chamel, N. Entrainment in Superfluid Neutron-Star Crusts: Hydrodynamic Description and Microscopic Origin. *J. Low Temp. Phys.* **2017**, *189*, 328–360. [CrossRef]
37. Andersson, N.; Glampedakis, K.; Ho, W.C.G.; Espinoza, C.M. Pulsar Glitches: The Crust is not Enough. *Phys. Rev. Lett.* **2012**, *109*, 241103. [CrossRef] [PubMed]
38. Chamel, N. Crustal Entrainment and Pulsar Glitches. *Phys. Rev. Lett.* **2013**, *110*, 011101. [CrossRef]
39. Montoli, A.; Antonelli, M.; Haskell, B.; Pizzochero, P. Statistical Estimates of the Pulsar Glitch Activity. *Universe* **2021**, *7*, 8. [CrossRef]
40. Montoli, A.; Antonelli, M.; Pizzochero, P.M. The role of mass, equation of state, and superfluid reservoir in large pulsar glitches. *Mon. Not. R. Astron. Soc.* **2020**, *492*, 4837–4846. [CrossRef]
41. Haskell, B.; Khomenko, V.; Antonelli, M.; Antonopoulou, D. Crust or core? Insights from the slow rise of large glitches in the Crab pulsar. *Mon. Not. R. Astron. Soc.* **2018**, *481*, L146–L150. [CrossRef]

42. Montoli, A.; Antonelli, M.; Magistrelli, F.; Pizzochero, P.M. Bayesian estimate of the superfluid moments of inertia from the 2016 glitch in the Vela pulsar. *Astron. Astrophys.* **2020**, *642*, A223. [CrossRef]
43. Sourie, A.; Chamel, N. Force on a neutron quantized vortex pinned to proton fluxoids in the superfluid core of cold neutron stars. *Mon. Not. R. Astron. Soc.* **2020**, *493*, 382–389. [CrossRef]
44. Gügercinoğlu, E.; Alpar, M.A. Vortex Creep Against Toroidal Flux Lines, Crustal Entrainment, and Pulsar Glitches. *Astrophys. J. Lett.* **2014**, *788*, L11. [CrossRef]
45. Sourie, A.; Chamel, N. Vortex pinning in the superfluid core of neutron stars and the rise of pulsar glitches. *Mon. Not. R. Astron. Soc.* **2020**, *493*, L98–L102. [CrossRef]
46. Pizzochero, P.M.; Montoli, A.; Antonelli, M. Core and crust contributions in overshooting glitches: The Vela pulsar 2016 glitch. *Astron. Astrophys.* **2020**, *636*, A101. [CrossRef]
47. Ciolfi, R. Modelling the magnetic field configuration of neutron stars. *Astron. Nachrichten* **2014**, *335*, 624. [CrossRef]
48. Lander, S.K. Magnetic Fields in Superconducting Neutron Stars. *Phys. Rev. Lett.* **2013**, *110*, 071101. [CrossRef] [PubMed]
49. Sur, A.; Haskell, B. The impact of superconductivity and the Hall effect in models of magnetised neutron stars. *Publ. Astron. Soc. Austr.* **2021**, *38*, e043. [CrossRef]
50. Sur, A.; Cook, W.; Radice, D.; Haskell, B.; Bernuzzi, S. Long-term general relativistic magnetohydrodynamics simulations of magnetic field in isolated neutron stars. *Mon. Not. R. Astron. Soc.* **2022**, *511*, 3983–3993. [CrossRef]
51. Ruderman, M.; Zhu, T.; Chen, K. Neutron Star Magnetic Field Evolution, Crust Movement, and Glitches *Astrophys. J.* **1998**, *492*, 267–280. [CrossRef]
52. Ciolfi, R.; Rezzolla, L. Twisted-torus configurations with large toroidal magnetic fields in relativistic stars. *Mon. Not. R. Astron. Soc.* **2013**, *435*, L43–L47. [CrossRef]
53. Jones, D.I. Gravitational wave emission from rotating superfluid neutron stars. *Mon. Not. R. Astron. Soc.* **2010**, *402*, 2503–2519. [CrossRef]
54. Andersson, N.; Comer, G.L. Relativistic fluid dynamics: Physics for many different scales. *Living Rev. Relativ.* **2021**, *24*, 3. [CrossRef]
55. Haskell, B.; Sedrakian, A. Superfluidity and Superconductivity in Neutron Stars. In *The Physics and Astrophysics of Neutron Stars*; Rezzolla, L., Pizzochero, P., Jones, D.I., Rea, N., Vidaña, I., Eds.; Astrophysics and Space Science Library; Springer Nature: Cham, Switzerland, 2018; Volume 457, p. 401. [CrossRef]
56. Gavassino, L.; Antonelli, M. Thermodynamics of uncharged relativistic multifluids. *Class. Quantum Gravity* **2020**, *37*, 025014. [CrossRef]
57. Graber, V.; Cumming, A.; Andersson, N. Glitch rises as a test for rapid superfluid coupling in neutron stars. *ArXiv* **2018**, arXiv:astro-ph.HE/1804.02706.
58. Celora, T.; Khomenko, V.; Antonelli, M.; Haskell, B. The effect of non-linear mutual friction on pulsar glitch sizes and rise times. *Mon. Not. R. Astron. Soc.* **2020**, *496*, 5564–5574. [CrossRef]
59. Charbonneau, J.; Zhitnitsky, A. Novel mechanism for type I superconductivity in neutron stars. *Phys. Rev. C* **2007**, *76*, 015801. [CrossRef]
60. Link, B. Instability of superfluid flow in the neutron star core. *Mon. Not. R. Astron. Soc.* **2012**, *421*, 2682–2691. [CrossRef]
61. Sedrakian, A.; Clark, J.W. Superfluidity in nuclear systems and neutron stars. *Eur. Phys. J. A* **2019**, *55*, 167. [CrossRef]
62. Leinson, L.B. Vortex lattice in rotating neutron spin-triplet superfluid. *Mon. Not. R. Astron. Soc.* **2020**, *498*, 304–309. [CrossRef]
63. Pili, A.G.; Bucciantini, N.; Del Zanna, L. General relativistic models for rotating magnetized neutron stars in conformally flat space-time. *Mon. Not. R. Astron. Soc.* **2017**, *470*, 2469–2493. [CrossRef]
64. Castillo, F.; Reisenegger, A.; Valdivia, J.A. Magnetic field evolution and equilibrium configurations in neutron star cores: The effect of ambipolar diffusion. *Mon. Not. R. Astron. Soc.* **2017**, *471*, 507–522. [CrossRef]
65. Sur, A.; Haskell, B.; Kuhn, E. Magnetic field configurations in neutron stars from MHD simulations. *Mon. Not. R. Astron. Soc.* **2020**, *495*, 1360–1371. [CrossRef]
66. Pili, A.G.; Bucciantini, N.; Del Zanna, L. Axisymmetric equilibrium models for magnetized neutron stars in General Relativity under the Conformally Flat Condition. *Mon. Not. R. Astron. Soc.* **2014**, *439*, 3541–3563. [CrossRef]
67. Khomenko, V.; Antonelli, M.; Haskell, B. Hydrodynamical instabilities in the superfluid interior of neutron stars with background flows between the components. *Phys. Rev. D* **2019**, *100*, 123002. [CrossRef]
68. Andersson, N.; Glampedakis, K.; Haskell, B. Oscillations of dissipative superfluid neutron stars. *Phys. Rev. D* **2009**, *79*, 103009. [CrossRef]
69. van Eysden, C.A.; Melatos, A. Gravitational radiation from pulsar glitches. *Class. Quantum Gravity* **2008**, *25*, 225020. [CrossRef]
70. Sidery, T.; Passamonti, A.; Andersson, N. The dynamics of pulsar glitches: Contrasting phenomenology with numerical evolutions. *Mon. Not. R. Astron. Soc.* **2010**, *405*, 1061–1074. [CrossRef]
71. Thorne, K.S. Multipole expansions of gravitational radiation. *Rev. Mod. Phys.* **1980**, *52*, 299–339. [CrossRef]
72. Riley, T.E.; Watts, A.L.; Bogdanov, S.; Ray, P.S.; Ludlam, R.M.; Guillot, S.; Arzoumanian, Z.; Baker, C.L.; Bilous, A.V.; Chakrabarty, D.; et al. A NICER View of PSR J0030+0451: Millisecond Pulsar Parameter Estimation. *Astrophys. J. Lett.* **2019**, *887*, L21. [CrossRef]
73. Raaijmakers, G.; Greif, S.K.; Hebeler, K.; Hinderer, T.; Nissanke, S.; Schwenk, A.; Riley, T.E.; Watts, A.L.; Lattimer, J.M.; Ho, W.C.G. Constraints on the Dense Matter Equation of State and Neutron Star Properties from NICER's Mass-Radius Estimate of PSR J0740+6620 and Multimessenger Observations. *Astrophys. J. Lett.* **2021**, *918*, L29. [CrossRef]

74. Jones, P.B. The Alignment of the Crab Pulsar Magnetic Axis. *Ap&SS* **1975**, *33*, 215–230. [CrossRef]
75. Easson, I.; Pethick, C.J. Stress tensor of cosmic and laboratory type-II superconductors. *Phys. Rev. D* **1977**, *16*, 275–280. [CrossRef]
76. Haskell, B.; Priymak, M.; Patruno, A.; Oppenoorth, M.; Melatos, A.; Lasky, P.D. Detecting gravitational waves from mountains on neutron stars in the advanced detector era. *Mon. Not. R. Astron. Soc.* **2015**, *450*, 2393–2403. [CrossRef]
77. Giliberti, E.; Cambiotti, G.; Antonelli, M.; Pizzochero, P.M. Modelling strains and stresses in continuously stratified rotating neutron stars. *Mon. Not. R. Astron. Soc.* **2020**, *491*, 1064–1078. [CrossRef]